

Incorporating structured assumptions with probabilistic graphical models in fMRI data analysis

Ming Bo Cai^{**a,b,*}, Michael Shvartsman^{**c}, Anqi Wu^{**d}, Hejia Zhang^{**e},
Xia Zhu^{**f}

^a*International Research Center for Neurointelligence (WPI-IRCN), UTIAS, The University of Tokyo, Japan*

^b*Princeton Neuroscience Institute, Princeton University, United States*

^c*Facebook Reality Labs, United States*

^d*Mortimer B. Zuckerman Mind Brain Behavior Institute, Columbia University, United States*

^e*Department of Electrical Engineering, Princeton University, United States*

^f*Intel Corporation, United States*

Abstract

With the wide adoption of functional magnetic resonance imaging (fMRI) by cognitive neuroscience researchers, large volumes of brain imaging data have been accumulated in recent years. Aggregating these data to derive scientific insights often faces the challenge that fMRI data are high dimensional, heterogeneous across people, and noisy. These challenges demand the development of computational tools that are tailored both for the neuroscience questions and for the properties of the data. We review a few recently developed algorithms in various domains of fMRI research: fMRI in naturalistic tasks, analyzing full-brain functional connectivity, pattern classification, inferring representational similarity and modeling structured residuals. These algorithms all solve the challenges in fMRI by resorting to the same solution: they start from making clear statements of assumptions about neural data and existing domain knowledge, incorporating those assumptions and domain knowledge into probabilistic graphical models, and using those models to estimate properties of interest or latent structures in the data. Such

*Corresponding author: mingbo.cai@ircn.jp

**All authors contributed equally.

© 2020. This manuscript version is made available under the CC-BY-NC-ND 4.0 license <http://creativecommons.org/licenses/by-nc-nd/4.0/>

approaches can avoid erroneous findings, reduce the impact of noise, better utilize known properties of the data, and aggregate data across groups of subjects. With these successful cases, we advocate wider adoption of explicit model construction in cognitive neuroscience. Although we focus on fMRI, the principle illustrated here is generally applicable to brain data of other modalities.

Keywords: probabilistic graphical model, Bayesian, fMRI, cognitive neuroscience, big data, factor model, matrix normal

1. Introduction

Functional magnetic resonance imaging (fMRI) [1, 2] is a powerful tool to study the brain’s activity and functions. The fluctuation of the fMRI signal is related to the fluctuation of the concentrations of the oxygenated and deoxygenated hemoglobin in the blood, which follows the increase or decrease of local neuronal activity with a delay[3, 4]. This relation to the neural activity, together with its non-invasive nature, full brain coverage and reasonable balance between spatial and temporal resolution, makes fMRI a widely used brain imaging technique for studying the neural correlates of perceptual and cognitive processes in humans.

Early fMRI studies focused on identifying the brain regions specifically activated when certain perceptual or cognitive processes are engaged. Most of the widely used fMRI analysis packages [5–7] were originally developed primarily in service of this goal of functional localization. Due to individual differences in brain structure, head motion during experiments and the existence of various artifacts, many steps of preprocessing are needed for the fMRI data to be properly analyzed. These include motion correction, slice-timing correction and alignment between functional and structural MRI images. New denoising methods continue to be developed [8–11], providing many options to suppress noise and artifacts. As a result, all of these software packages are modular: each module performs one unique type of processing or analysis on its input data. It becomes a common practice to compose an analysis pipeline by stacking modules one after another. Data flow through the pipeline, such that the output from one or more modules become input data to another module. In such an approach, a researcher might perceive a sense of assurance that after each data processing procedure, certain type of noise or artifact has been removed, or certain quantities of interest have

been correctly estimated (for example, estimating voxel-wise activation by different task conditions using the general linear model, or GLM [12]). Researchers then often move on to the next stage of *data mining* by applying various machine learning tools or further compose analysis procedures using the results generated from early stages of processing as input. The popularity of this workflow is such that several tools have been developed specifically to facilitate building pipelines by mixing and matching modules from different packages [13, 14]. Benefits of such pipelines include wider adoption of robust pipelines and easy validation of published results. While modularity is a good programming principle and pipelining analyses is a common practice, recent work has pointed out that during sequential applications of analysis or filtering steps on the data, later steps may reintroduce artifacts intended to be removed by early steps [15]. Similar to this phenomenon, it has also been shown that when directly taking the output of early processing steps (such as the estimation of the activation pattern to each task condition) as input to representational similarity analysis (RSA), the correlation of noise inherent in the output of GLM can in fact create spurious similarity structure in the RSA result [16–18]. In functional connectivity analysis, it was also found that various denoising procedures can introduce spurious brain network correlational structures [19–23]. These findings illustrate one practical drawback of the pipelining approach: individual steps of procedures may not be compatible in their assumptions, leading to potential adverse interaction among procedures.

In this article, we argue that instead of taking a data mining approach towards neural imaging analysis by composing various data processing procedures, a model-based approach is more transparent and often more accurate. In this approach, a probabilistic model of how the quantities of interest directly or indirectly generate the measured data stands in the center of the analysis. By focusing on the model, assumptions about data becomes more transparent to developers and users.

As illustrated in Figure 1, such approach typically involves four major steps. The first step is defining the problem: deciding what question is asked or what problem needs to be solved, and deciding what quantity allows one to answer the question or to characterize certain aspect of the brain. After the question is clearly defined, the second step is to make explicit assumptions of how the quantity of interest and experimental manipulations directly or indirectly contribute to the data to be analyzed, and to make assumptions of how variables of no interest (nuisance factors) may jointly impact the data.

If there is domain knowledge of the properties of fMRI data that can help constructing models of fMRI, it should be clearly stated at this step as well. The third step is to translate these assumptions and domain knowledge into a computational model. Such computational models can often be described by probabilistic graphical models [24] composed of nodes and directed edges between nodes. When building probabilistic graphical models, the data, experimental manipulation, quantity of interest and nuisance factors that are considered in the assumptions of the previous step all become variables (either known or unknown) and are each represented by a node in the graph. The hypothesized relations between variables in the models are expressed as conditional probability of one variable given one or more other variables and are represented by directed edges. Each edge is directed from one variable to another variable that is conditioned on it. The domain knowledge is either captured by the prior distribution of certain variables in the graph, or in the form of the conditional dependencies. The probabilistic nature of such models is a natural choice for capturing the noise properties in the system and the potential uncertainty in the estimates from the researchers' perspective. Once the probabilistic graphical model is built, the fourth step is to deploy computational techniques to estimate the unknown variables of interest in the model. This step essentially inverts the model by inferring variables of interest at the source of the directed edges in the graphical model. In some cases, inferring these variables serves to answer the original question by providing characterization of some aspect of brain activity. In other cases, when the scientific question is to test competing hypotheses, the competing hypotheses should be translated into probabilistic graphical models that differ in either the range of values of some key variables or in the structures of the models. The selection of the winning model can be either based on classical statistical tests of the inferred values of the key variables, or based on the likelihood that each model can give rise to the data, marginalizing unknown variables (model evidence). To approximate posterior distributions of latent variables (variables that are directly or indirectly causal to nodes representing observable data) in the probabilistic graphical models, techniques such as Markov Chain Monte Carlo (MCMC) or variational Bayes are often employed. In certain cases, when the posterior distribution of these latent variables given the observed data can be analytically derived, exact inference of the posterior distribution or the *maximum a posteriori* values of the variables can often be achieved. A full discussion of the inference methods is out of the scope of this paper. Interested readers may refer to tutorials such as Chapter 8 of

[25] or part II of [24].

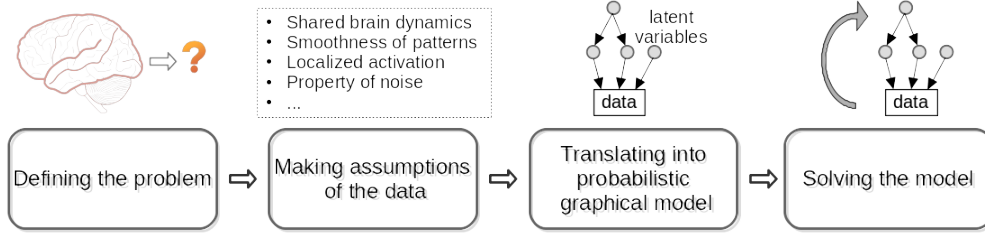


Figure 1: The model-based approach to analyze neural data. In general, this involves four steps: (1) clearly defining the problem to solve or the question being asked; (2) making assumptions about the property of the data, including domain knowledge and causal relation between latent variables and measured data; (3) Translating these assumptions to a probabilistic graphical model which expresses how latent variables together generate measured data. The model uses conditional probability distribution between variables to capture their causal relations; (4) solving the model to infer latent variables or to draw conclusion for the question asked in the first step.

In the model-based approach described above, because a probabilistic graphical model is explicitly built, it is easy to evaluate whether the inference procedure can reliably recover the variables of interest in the model, by simulating data according to the model and comparing the recovered values of those variables with the values used in the simulation. In contrast, the traditional approach which merely stacks analysis procedures without building an explicit model of the data generating process lacks the ability to simulate data in accordance with its (implicit) assumptions. Without simulating data, it becomes impossible to verify an analysis can yield correct result, because researchers are only left with real neural data of which the generative process is not known. Thus, there is no guarantee that the quantity extracted by such analysis bears direct relation to what the researchers are interested in.

In addition to transparency and verifiability, the model-based approach offers the flexibility to combine the advantage of various pieces of domain knowledge of the brain (for example, brain activation patterns tend to be spatially smooth). This is because domain knowledge can be translated into a prior distribution of certain form over some latent variables in the probabilistic graphical model. With the probabilistic graphical model as a backbone, different prior distributions may act as add-on parts that can be plugged in at different places of the model depending on what domain knowledge is proper for the purpose of analysis. For example, in 2.2, we show that the smoothness

assumption of the brain activity and the similarity of brain networks across people are incorporated in the Gaussian shape of the spatial basis for brain patterns and the Gaussian distribution of node location across subjects, respectively. In 2.3, we show that two types of prior knowledge about fMRI decoding weights can also be incorporated together by assuming a Gaussian Process prior on the joint distribution of the fMRI decoding weights of all voxels.

In the following, we select example analysis methods developed in different domains to illustrate how the model-based approach to neural imaging data can be applied to discovering shared neural dynamics across participants doing the same task, modeling the functional connectivity among voxels, improving the performance of decoding mental contents and obtaining interpretable decoding weights, reducing the bias in estimating similarity among activation patterns, and providing more comprehensive model of the noise in fMRI data. These methods also illustrate how the probabilistic graphical model[24], which stands at the center of all the methods, can accommodate domain knowledge and known properties of the data and facilitate aggregating information over larger datasets. These features allow us to mitigate the limitations in fMRI data: high dimensionality (many voxels), low sample size in single participant, heterogeneity across participants and high noise.

Because the focus is on illustrating the principle of model-based approach, this paper can by no means provide a thorough review of all model-oriented methods of fMRI analysis. Readers are encouraged to also refer to several other reviews (e.g., [26, 27]) on Bayesian approaches to fMRI for a more comprehensive understanding of other existing model-based tools that also share the advantages illustrated here.

2. Examples of model-based analysis methods for fMRI data

2.1. *Discovering latent neural dynamics for naturalistic task*

- *Defining the problem: aggregating multi-subject fMRI data*

The fMRI datasets with naturalistic stimuli, such as movies or audiobooks, usually have limited number of samples per subject. In general, fMRI datasets not only have a large number of voxels but also tends to have a small number of time points due to the limitation of samples per experiment session as a result of the slowness of haemodynamic response and limited sample rate of the scanner. In fMRI datasets with naturalistic stimuli, it is also infeasible

to collect many samples from a single subject in many cases when the experiments require the natural stimulus to be fresh to the subjects, so each subject could only be exposed to the same stimulus once. Therefore, to improve analysis sensitivity, we need to aggregate data from multiple subjects with the same stimulus effectively. The idea is similar to repeated measures designs in neuroscience where the same variable is measured multiple times, but here the repetition is over different subjects. In our fMRI analysis application, essentially, we want to find what is common across subjects. The challenge is that the anatomical and functional structures between subjects are not aligned [28]. For example, when listening to the same music, a musician and a person without any music training will probably have different responses. Some early attempts applied pipelines such as averaging the fMRI data from all subjects after anatomical alignment, which essentially assumes voxels of different brains have one-to-one correspondence [28, 29]. In contrast, Shared Response Model (SRM) [30] is a Bayesian factor analysis model that finds the shared latent neural dynamics across subjects in a multi-subject fMRI dataset after anatomical alignment, without assuming one-to-one voxel correspondence.

- *Making assumptions: temporally-aligned stimulus*

SRM assumes that the stimulus in a naturalistic task dataset is temporally-aligned. That is, all the subjects receive the same stimulus at the same time point in the task. Therefore, we assume that all the subjects share the same low-dimensional latent representation within a dataset, called "shared response." On the other hand, to account for the differences between subjects, SRM assumes that each subject has a subject-specific spatial basis for generating the observed fMRI data from the shared response.

- *Translating assumptions to a graphical model: shared response as a latent variable*

To translate the assumptions above into a computational model, let us look at the deterministic SRM first and then the probabilistic version. The deterministic SRM factorizes the transpose of each subject's brain image data \mathbf{X}_m^T into a subject-specific spatial basis \mathbf{W}_m and the shared response \mathbf{S} with the orthogonal constraint $\mathbf{W}_m^T \mathbf{W}_m = I$ (Fig.2), where $\mathbf{X}_m \in \mathbb{R}^{T \times V_m}$ is the brain image data of subject m , $\mathbf{W}_m \in \mathbb{R}^{V_m \times K}$ is the subject-specific spatial basis of subject m , $\mathbf{S} \in \mathbb{R}^{K \times T}$ is the shared response across subjects, V_m is the number of voxels of subject m , T is the number of time points, and K is the number of features. K is a tunable hyper-parameter which is usually

much smaller than T . More formally, SRM minimizes the Frobenius norm of reconstruction error

$$\|\mathbf{X}_m^T - \mathbf{W}_m \mathbf{S}\|_F^2 \quad (1)$$

under the constraint $\mathbf{W}_m^T \mathbf{W}_m = \mathbf{I}$. This simple model is then extended to a probabilistic setting, as shown in Fig.2. Here $x_{mt} \in \mathbb{R}^{V_m}$ denotes the observed brain image data of subject m at time t , $s_t \in \mathbb{R}^K$ denotes a shared latent random vector with

$$s_t \sim \mathcal{N}(0, \Sigma_s). \quad (2)$$

The distribution of x_{mt} conditioned on s_t is then

$$x_{mt}|s_t \sim \mathcal{N}(\mathbf{W}_m s_t + \mu_m, \rho_m^2 \mathbf{I}), \quad (3)$$

where the subject-specific mean μ_m accounts for non-zero mean and $\rho_m^2 \mathbf{I}$ is the subject dependent isotropic noise covariance. In the probabilistic version, the orthogonal constraint still holds. A constrained expectation-maximization (EM) algorithm is used to solve this model.

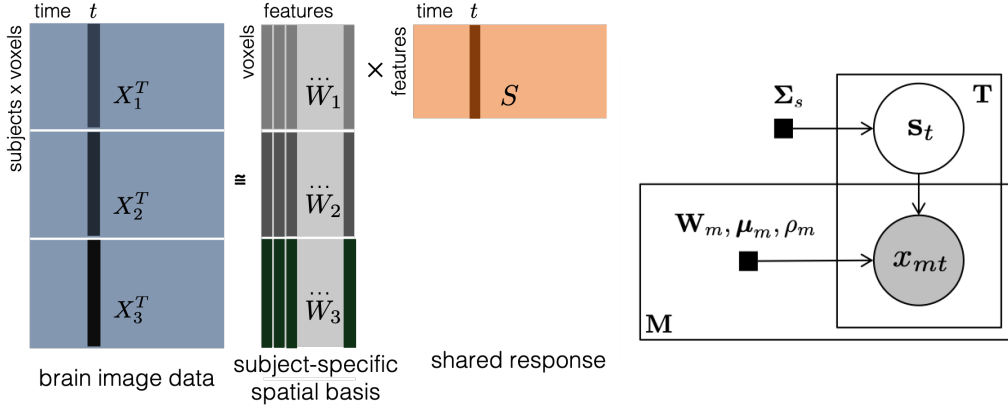


Figure 2: **Left:** Illustration of deterministic SRM for three subjects. **Right:** Graphical model for SRM with M subjects and T time points. Brain image data $x_{mt} \in \mathbb{R}^{V_m}$ (V_m voxels) is observed from subject m at time t , $t = 1 : T, m = 1 : M$. Each observation x_{mt} is a linear combination of subject-specific orthogonal basis (columns of \mathbf{W}_m) using the weights specified by s_t . The two plates are repeated T and M times, respectively. Shaded nodes: observations, unshaded nodes: latent variables, and black squares: parameters.

- Applications: identified shared responses and extensions

The SRM model identifies the shared and individual responses in a multi-subject fMRI dataset with naturalistic tasks. The extracted shared responses

allow us to aggregate information from multiple subjects, and the individual responses could be used to identify what is unique for each subject. SRM shows improved performance in various tasks, such as image-viewing fMRI data classification, using shared and individual responses, as described in [30], and movie scene classification[31]. Compared with hyperalignment (HA) [32], SRM also has a built-in dimensionality reduction mechanism with a tunable number of features, where HA is an earlier multi-subject alignment algorithms with the objective to minimize

$$\|\mathbf{W}_m^T \mathbf{X}_m^T - \mathbf{S}\|_F^2 \quad (4)$$

under the constraint $\mathbf{W}_m^T \mathbf{W}_m = I$, $\mathbf{W}_m \in \mathbb{R}^{V_m \times V_m}$. Furthermore, SRM already has several extensions which make it more useful. For example, searchlight SRM [33] combines SRM with searchlight analysis, which enables the localization of shared responses. Multi-dataset multi-subject analysis (MDMS) [34] extends SRM to the multi-dataset setting where the model can aggregate information across subjects and datasets with different stimuli. Semi-supervised SRM [35] combines SRM with an additional multinomial logistic regression objective, such that the model can leverage partially labeled data.

2.2. Discovering full-brain functional connectivity from fMRI

- Defining the problem: discovering full-brain functional connectivity

Recent research suggests that the functional connectivity (networks) in human brain, commonly represented by the spatial covariance structure of fMRI data, can change during different cognitive states [36]. To estimate functional connectivity during a particular cognitive state (or an experimental condition) from fMRI data, one approach is to compute the correlation between the time series of pairs of voxels [37]. Because of the computational time and memory demand by this voxel-based approach, most researchers focus their analysis on pre-selected regions of interest (ROIs). Topographic Factor Analysis (TFA) and Hierarchical Topographic Factor Analysis (HTFA) are Bayesian factor analysis models that were proposed to efficiently discover full-brain function connectivity in large multi-subject neuroimaging datasets [38].

- Making assumptions: spatial function-based latent factors

Both TFA [39] and HTFA [38] cast each subject's brain images as a linear

combination of latent factors, where each latent factor is modeled as a parameterizable spatial function. Each latent factor can be interpreted as a node in a simplified representation of the brain’s network. A subject’s matrix of the changing weights on the nodes over time may be viewed as a low-dimensional embedding (or representation) of the original brain data. The pairwise correlations between each factor’s weights over time further reflect the signs and strengths of the node-to-node connections (i.e. the functional connectivity). Both TFA and HTFA approximate each subject’s functional connectivity by firstly representing each brain image in terms of the activities of a set of localized network nodes, and then computing the covariance of the activity. Furthermore, HTFA [38] is a multi-subject extension of TFA [39], and attempts to discover the network nodes that are common across a group of subjects. HTFA estimates a global template as well as each individual’s subject-specific template. The global template describes where each common network node is placed, how wide it is and how active it tends to be. Each subject-specific template is a particular instantiation of the common network nodes and the subject’s node activities. The hierarchical global and subject-specific template enables HTFA for conducting inter-subject functional connectivity (ISFC) analyses.

- *Translating assumptions to a graphical model: global and subject specific template*

HTFA is formulated as a probabilistic latent variable model. Let $\mathbf{X}_m \in \mathbb{R}^{T_m \times V_m}$ represent subject m ’s data as a matrix with T_m fMRI samples of the activity of V_m voxels, each sample being vectorized as one row in \mathbf{X}_m . Then, each subject is approximated with a factor analysis model

$$\mathbf{X}_m = \mathbf{W}_m \mathbf{F}_m + \mathbf{E}_m, \quad (5)$$

where $\mathbf{W}_m \in \mathbb{R}^{T_m \times K}$ are the weights of $\mathbf{F}_m \in \mathbb{R}^{K \times V_m}$, the latent factors. Each latent factor (row of \mathbf{F}_m) is a radial basis function (RBF) with center at $\mu_{m,k}$ and width $\lambda_{m,k}$

$$f_{m,k}(\mathbf{p}; \mu_{m,k}, \lambda_{m,k}) = \exp \left\{ -\frac{\|\mathbf{p} - \mu_{m,k}\|_2^2}{\lambda_{m,k}} \right\}, \quad (6)$$

in positions $\mathbf{p} \in \mathbb{R}^3$ for all the voxels in the three-dimensional voxel space of the brain. HTFA defines the local factors in \mathbf{F}_m as perturbations of the factors of a global template in \mathbf{F} . Therefore, the factor centers $\mu_{m,k}$ for all subjects are obtained from a multivariate normal distribution with mean

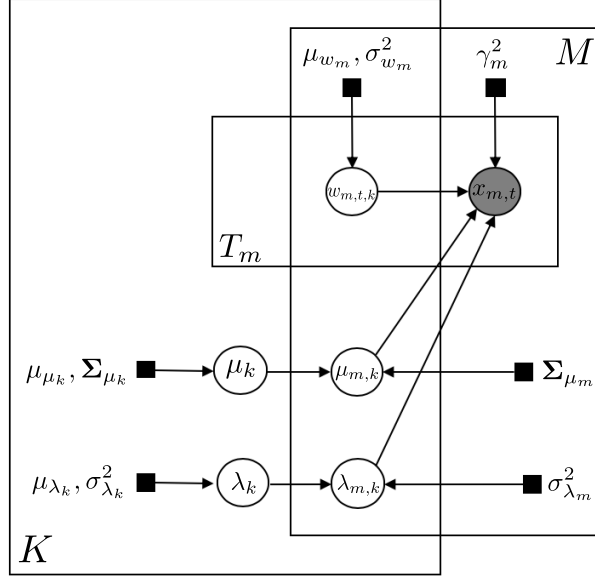


Figure 3: Graphical model for HTFA. Brain image data $x_{m,t} \in \mathbb{R}^{V_m}$ (V_m voxels) is observed from subject m at time t , $t = 1 : T_m, m = 1 : M$. Each observation $x_{m,t}$ is a linear combination of K number of subject-specific latent factors, using the weights specified by $w_{m,t,k}$. Each latent factor (row of F_m) is a spatial function of $\mu_{m,k}$ and $\lambda_{m,k}$. The three plates are repeated K, T_m and M times, respectively. Shaded nodes: observations, unshaded nodes: latent variables, and black squares: parameters.

μ_k and covariance Σ_{μ_m} . The mean μ_k represents the center of the global k^{th} factor, while Σ_{μ_m} determines the distribution of the possible distance between the global and the local center of the factor. Similarly, the widths $\lambda_{m,k}$ for all subjects are drawn from a normal distribution with mean λ_k , the width of the global k^{th} factor, and variance $\sigma_{\lambda_m}^2$. The model defines multivariate Gaussian prior $\mathcal{N}(\mu_{\mu_k}, \Sigma_{\mu_k})$ for the global parameters μ_k and Gaussian prior $\mathcal{N}(\mu_{\lambda_k}, \sigma_{\lambda_k}^2)$ for λ_k , respectively. In addition, the columns of the weight matrices \mathbf{W}_m are modeled with a $\mathcal{N}(\mu_{w_m}, \sigma_{w_m}^2)$ distribution and the elements in the noise term \mathbf{E}_i are assumed to be independent with a $\mathcal{N}(0, \gamma_m^2)$ distribution. The associated graphical model is shown in Fig. 3.

- Solving the model

The *maximum a posteriori* (MAP) probability estimation procedure is used to solve the HTFA model. The method consists of a global and local step that iteratively update the parameters. The global step updates the parameters

of the K distributions in the global template. The local step updates for each subject m the weight matrices \mathbf{W}_m , the local centers $\mu_{m,k}$ and the widths $\lambda_{m,k}$ of each latent factor. To update the parameters of the factors in \mathbf{F}_m , the local step solves the following problem, where ϕ_m is a subsampling coefficient.

$$\begin{aligned} \left\{ \hat{\mu}_{m,k}, \hat{\lambda}_{m,k} \right\}_k = \operatorname{argmin}_{\{\mu_{m,k}, \lambda_{m,k}\}_k} & \frac{1}{2\sigma_m^2} \|\mathbf{X}_m - \mathbf{W}_m \mathbf{F}_m\|_F^2 \\ & + \frac{1}{2\phi_m} \sum_{k=1}^K (\mu_{m,k} - \hat{\mu}_k) \boldsymbol{\Sigma}_{\mu_k}^{-1} (\mu_{m,k} - \hat{\mu}_k)^T \\ & + \frac{1}{2\phi_m \sigma_\lambda^2} \sum_{k=1}^K (\lambda_{m,k} - \hat{\lambda}_k)^2 \end{aligned} \quad (7)$$

Eq. (7) consists of reconstruction error, the Mahalanobis distance between global and local centers, and the Euclidean distance between global and local widths. Due to its non-linearity, the latent factors in local template are computed using a non-linear least squares solver, and implemented with a trust-region reflective method. The weight matrix is solved with a closed-form solution of the form of ridge regression. The hyper-parameters of the global template are updated given the local estimates and under the assumption that the posterior has a conjugate prior with multivariate normal and normal distribution for centers and width, respectively.

- *Advantages*

Because the number of network nodes is typically substantially smaller than the number of fMRI voxels, one obvious advantage of HTFA is that it can be orders of magnitude more efficient than traditional voxel-based functional connectivity approaches. Compared to other dimensionality reduction methods, HTFA provides additional advantages: (a) it provides estimation of both global and subject-specific templates, and builds connections between them; (b) the spatial function of latent factors allows network nodes to be overlapping rather than forcing them to be completely distinct, as would be the case of functional connectivity based on anatomically defined brain region segmentation; (c) it provides a natural means of determining how many network nodes (latent factors) should be used for a given dataset (further details about determining K can be acquired from [38]); and (d) because HTFA decomposes brain images into sums of spatial functions, it supports seamless mapping between images of different resolutions and potentially different

imaging modalities.

2.3. Obtaining interpretable decoding weights on fMRI patterns

- Defining the problem: fMRI decoding with sparsity

A primary research problem neuroscientists have been studying with fMRI is brain decoding or inverse inference [40–42]. The goal of a decoding task is to understand how brain activity can predict task-related variables, e.g. reaction time or object category. Researchers often use linear classification and regression methods to identify the brain regions or voxels that are most related to these task-related variables by inspecting the decoding weights.

A piece of domain knowledge with fMRI decoding is that only few small regions of the brain are specifically activated during an individual task because different regions of the brain are specialized to different functions. In the linear regression methods that are common in the field, this assumption is equivalent to assuming that the weights mapping fMRI to task-related variables are mostly zeros with a few non-zero values, which is referred to as “sparsity”. This model assumption is also reasonable from a statistical standpoint, since the task variable is linked to fMRI with usually tens of thousands of voxels, but the number of fMRI volumes with valid task labels is far smaller, e.g. a few hundreds. We need to estimate tens of thousands of coefficients to map a full brain pattern down to a single task variable given only a few hundreds of observations. This is referred to as a high-dimensional and small-sample issue, where the linear regression model would fit seemingly predictive information from noise instead of the underlying brain signal, and thus doesn’t generalize well to new data. To address this issue, one can reduce the number of coefficients. With the sparsity assumption, we effectively regularize the linear decoding model by restricting the weight parameter space to a much smaller one, thus mitigating the issue.

- Making assumptions: region sparsity

Sparse decoding has already been exploited in the previous literature [43–45]. However, the non-zero coefficients are not randomly distributed throughout the brain, but tend to arise in clusters, and are therefore not independent a priori. Sets of voxels allowing to discriminate between different brain states are expected to form small localized and connected areas. If one voxel encodes information related to the task, its neighbor voxels should carry similar information, given that contiguous brain regions of shared functions extend over

multiple adjacent voxels. This type of sparsity is referred to as “region sparsity” [46]. By considering such region sparsity, one can impose a structured sparsity regularization over the decoding weights which further constrains the parameter space to search and thus eases the decoding weights optimization task. Wu et al. [46] developed a Bayesian framework that incorporated such region sparsity into brain decoding for fMRI analysis and showed the superior decoding performance and interpretable decoding weights for three brain imaging datasets.

- *Translating assumptions to a graphical model: building a region sparsity prior over the brain weights*

The model proposed in [46] is referred to as “Dependent Relevance Determination” (DRD). It builds a Bayesian hierarchical model that imposes a sparsity prior over the decoding weights. Unlike previous work with sparsity assumptions, DRD also assumes that nearby sparse voxel-activation events should be correlated to each other based on their spatial locations.

Formally, the fMRI decoding problem can be formulated in a linear regression setting: at time t , consider a scalar response $y_t \in \mathbb{R}$ linked to an input vector $\mathbf{x}_t \in \mathbb{R}^V$ via the linear model:

$$y_t = \mathbf{x}_t^\top \mathbf{w} + \epsilon_t, \quad \text{for } t = 1, 2, \dots, T, \quad (8)$$

with observation noise $\epsilon_t \sim \mathcal{N}(0, \sigma^2)$, where T is the number of time points and V is the number of voxels. The regression (linear weight) vector $\mathbf{w} \in \mathbb{R}^V$ is the quantity of interest. We can denote the fMRI data matrix by $\mathbf{X} \in \mathbb{R}^{T \times V}$, where each row of \mathbf{X} is the t^{th} input vector \mathbf{x}_t^\top and $T \ll V$, and the observation vector by $\mathbf{y} = [y_1, \dots, y_T]^\top \in \mathbb{R}^T$. Since the noise is Gaussian, it can be written as

$$\mathbf{y} | \mathbf{X}, \mathbf{w}, \sigma^2 \sim \mathcal{N}(\mathbf{y} | \mathbf{X}\mathbf{w}, \sigma^2 \mathbf{I}). \quad (9)$$

DRD imposes a zero-mean multivariate normal prior on \mathbf{w} :

$$\mathbf{w} | \boldsymbol{\theta} \sim \mathcal{N}(0, C(\boldsymbol{\theta})), \quad (10)$$

where the prior covariance matrix $C(\boldsymbol{\theta})$ is a function of hyperparameters $\boldsymbol{\theta}$. One can specify $C(\boldsymbol{\theta})$ based on prior knowledge on the regression vector, e.g. sparsity [47–49], smoothness [50, 51], or both [52]. Ridge regression assumes $C(\theta) = \theta^{-1} I$ where θ is a scalar for precision and I is the identity matrix. Automatic relevance determination (ARD) [53] uses a diagonal prior covariance

matrix with a distinct hyperparameter θ_i for each element of the diagonal, thus $C_{ii} = \theta_i^{-1}$. DRD is an extension of ARD by imposing dependency over θ_i .

Given the general Bayesian linear regression setting, DRD aims to construct a covariance $C(\boldsymbol{\theta})$ which generates the region-sparse \mathbf{w} . This is achieved by introducing a latent variable $\mathbf{u} \in \mathbb{R}^V$. \mathbf{u} is from a Gaussian process (GP) prior, i.e.

$$\mathbf{u} \sim \mathcal{N}(b\mathbf{1}, k). \quad (11)$$

A Gaussian process [54] is a stochastic process whose realizations are draws from a multivariate normal distribution, but whose mean b and covariance k can be functions of another input (e.g. spatial locations). For example, by defining a Gaussian process with covariance (kernel) that is a function of spatial distances, we can constrain covariance of draws from it to be constrained based on this information. Most commonly in GPs, the squared exponential kernel is used, which constrains the draws from the multivariate normal to be smooth over space, i.e. $k(\chi, \chi') = \rho \exp(-\frac{\|\chi - \chi'\|^2}{2l^2})$ where χ is the spatial location of a voxel. Functions sampled from such a GP are smooth functions. The smoothness is determined by the length scale $l \in \mathbb{R}$ and the magnitude of the functions is determined by $\rho \in \mathbb{R}$. These three hyperparameters in the DRD prior are jointly denoted by $\boldsymbol{\theta} = \{b, \rho, l\}$.

By imposing a GP prior over the latent \mathbf{u} , DRD effectively captures dependencies in \mathbf{u} , based on which Wu et al. formulate the covariance of \mathbf{w} with

$$C = \text{diag}[\exp(\mathbf{u})]. \quad (12)$$

The exponential function here ensures the non-negativity of values on the diagonal of C , which makes it a valid covariance. When the mean b is very negative, $\exp(\mathbf{u})$ has many close-to-zero values that result in soft-sparsity. Note that the spatial smoothness of \mathbf{u} induces dependencies between the variances of nearby voxels, that is, the prior variance changes slowly between neighboring coefficients. If the i^{th} coefficient of \mathbf{u} has a large prior variance, then probably the coefficients of its adjacent voxels are large as well.

Fig. 4A and B show the probabilistic graphical model of DRD and the process to generate region-sparse samples for \mathbf{w} . Given a smooth kernel k , DRD first generates a smooth function for \mathbf{u} with some negative mean b . Exponentiating it gives rise to a nonnegative function \mathbf{g} which has a few nonzero bumps and largely zeros. The covariance C is then formulated by putting \mathbf{g} on the diagonal of the covariance matrix. Finally region-sparse

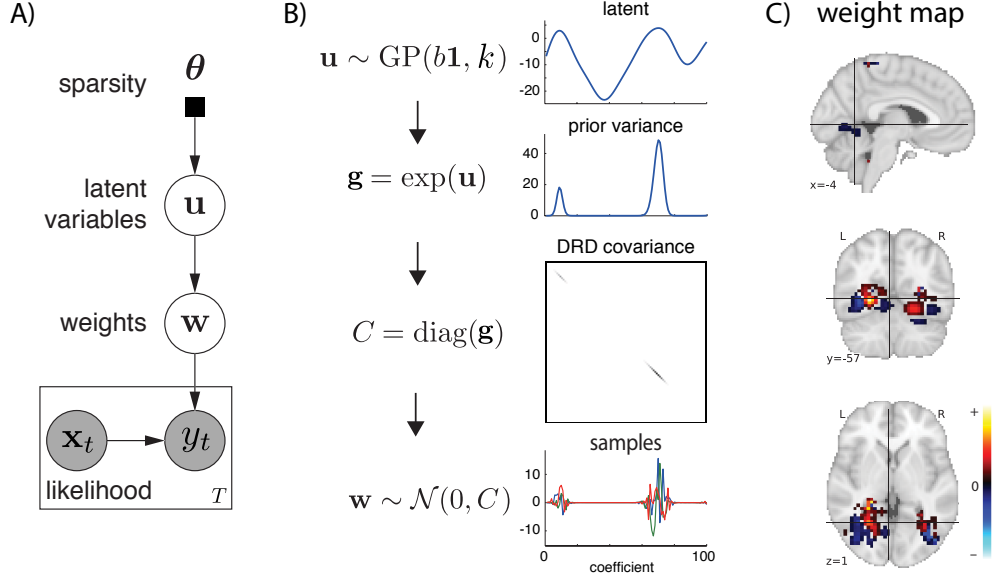


Figure 4: A) Probabilistic graphical model for DRD. The rectangular box indicates a graph for each time point. Each fMRI slice \mathbf{x}_t is mapped to the experimental response y_t together with a global variable \mathbf{w} (eq. 8). The decoding weight vector \mathbf{w} is conditioned on a latent variable \mathbf{u} (eq. 10 and 12). The latent variable \mathbf{u} is generated from some hyperparameters in θ (eq. 11). B) The generating process for region-sparse decoding weight \mathbf{w} . C) Interpretable decoding weight map for the house vs bottle pair. Yellow indicates very positive values and light blue indicates very negative values. Black means small values.

\mathbf{w} are sampled from a Gaussian prior with such a covariance. The region sparsity is achieved by 1) imposing dependence among nearby voxels; 2) squashing most values to approximately zeros via exponentiating negative values.

- Solving the model

In the paragraphs above, we show how to build a generative model for DRD to generate region-sparse decoding weights. When using DRD, one can apply it to fMRI decoding problems where we have the data \mathbf{X} and \mathbf{y} , and we aim to figure out what is the decoding weight vector \mathbf{w} . To solve this problem, we need to reverse the generating process using some inference methods. Exact Bayesian inference is infeasible with a DRD prior. However, approximate inference can be carried out efficiently using both Laplace approximation and Markov Chain Monte Carlo (MCMC) sampling. Further details regarding

inference can be acquired from [46].

- *Application: classification on a visual recognition task*

The visual recognition dataset [55] is from a study on object representation in human ventral temporal cortex. In the object recognition experiment, 6 subjects were asked to recognize 8 different types of objects (bottles, houses, cats, scissors, chairs, faces, shoes and scrambled control images). Wu et al. [46] examined this dataset to learn the weights mapping the fMRI brain activity to object categories for each subject. They cast the multi-category classification problems into multiple binary classification problems for each pair of categories. Wu et al. employed the same linear regression model as in eq. 8 for training the model. When making predictions, they took the sign of the output y as the discrete binary labels (+1/−1).

They showed that DRD achieved the highest accuracies for most of the binary classifications compared with other state-of-art sparse decoding methods [44, 45]. More specifically, DRD is able to find interpretable decoding weight maps for many pairs. Fig. 4C presents the brain map estimation for the house-vs-bottle pair. There are clustered positive decoding weights in the parahippocampal place area (PPA) (responding more strongly to scenes depicting places) [56] and clustered negative weights in the lateral occipital complex (LOC) (responding to objects in human occipito-temporal cortex) [57] discovered by DRD, which are not found by other sparse decoding methods.

We describe the DRD model here in a generative way. The brain decoding weights are generated from a DRD prior. But the application is a discriminative model, i.e. mapping fMRI data to experimental variables. Because the DRD prior was proposed to learn region-sparse brain weights regardless of whether a model is discriminative or generative, it can also be inserted to generative models such as the factor analysis models in SRM in essentially the same way.

2.4. *Inferring representational similarity between neural patterns*

- *Defining the problem: neural pattern similarity*

As sensory inputs get processed in the brain, each neural population of one brain region performs nonlinear computation of the input from neurons of other regions. The representation of the same external object thus changes from one region to another. One fundamental question in neuroscience is how these representations are transformed, in service for deciding the right

actions to take[58, 59]. One way to describe representation is in terms of what stimuli are encoded closer and what are encoded farther apart. Beyond studying representation of external stimuli, the same question can also be asked about different cognitive states: which states are represented closer in a brain region?

Early behavioral studies investigated representations of objects by asking people to judge how similar a pair of stimuli are to each other [60]. The structure of the similarity matrix, composed of the judged degrees of similarity between all pairs of tested stimuli, reflects the geometry of the internal representational space being used to encode stimuli. Such approach is limited to representations accessible for conscious report[61]. To overcome this and to compare computational models against multiple types of neural data, Kriegeskorte et al. [62] proposed Representational Similarity Analysis (RSA), which utilizes neural recordings to understand the structure of representations. This analysis assumes that the similarity between the neural patterns elicited by each pair of stimuli in a brain region reflects the similarity between the representations of these stimuli in that region. Because it does not rely on subjective judgment, RSA can be applied to study representation in any stage of sensory processing[63, 64]. Measuring similarity between neural activity patterns evoked by sensory stimuli or cognitive states is its central goal.

- *Making assumptions: relations of representational structure, neural patterns and fMRI data*

In order to infer the similarity between neural activity patterns, one needs to first make assumptions about the relations between the neural patterns and the recorded neural data, and between the similarity structure and the patterns.

The neural activity of a region (RSA typically focuses on single brain region instead of the whole brain) during a task can be considered as being generated by the sum of various spatial patterns, each being modulated by different time courses. In this sense, the basic assumption of fMRI data underlying RSA is also a factor model, as in SRM and (H)TFA (Fig. 5A). The difference here is that at least a subset of the modulation time courses are explicitly tied to when and how much the brain is engaged in each task condition, which are pre-defined by the researchers. The spatial pattern being modulated by each time course is the relative degree by which different voxels are activated by the task condition. In addition to the activity ex-

plained by the temporal modulation of these patterns, the data also contain unexplained fluctuation with both spatial and temporal correlation. Therefore, the similarity matrix one seeks to estimate is only indirectly related to the noisy fMRI data through unknown neural activity patterns and their modulation time courses predicted by the task.

There are many ways to define similarity. One way is based on the cosine of the angle between the vectors corresponding to activity patterns in the space spanned by the voxel activation levels, which is adopted by the algorithm of Bayesian RSA (BRSA) [16, 17]. Other common ways include correlation between demeaned patterns, and Euclidean distance or Mahalanobis distance between patterns (as measures of dissimilarity) [62, 65–67]. Here we focus on cosine of angle between patterns, which can be alternatively considered as correlation without demeaning patterns.

- *Translating assumptions to a graphical model: two-stage model of fMRI data with representational structure as latent variable*

Since the time course of a task is known, the modulation time course (so-called design matrix) can be constructed based on the timing of the task conditions and the shape of the smooth delayed response (the haemodynamic response function, HRF) in fMRI signals following neuronal activity. We denote the design matrix as $\mathbf{S} \in \mathbb{R}^{T \times K}$, where T is the total time points and K is the number of task conditions in an experiment, then the factor model of fMRI data can be expressed as

$$\mathbf{X} = \mathbf{S}\mathbf{W} + \mathbf{S}_0\mathbf{W}_0 + \mathbf{E} \quad (13)$$

Here, $\mathbf{X} \in \mathbb{R}^{T \times V}$ is the time by voxel matrix of the fMRI time series in a region of interest where V is the total number of voxels in that region. $\mathbf{W} \in \mathbb{R}^{K \times V}$ is the unknown activation patterns associated with all the task conditions. $\mathbf{S}_0\mathbf{W}_0$ captures spatially correlated fluctuation unrelated to the task. \mathbf{E} denotes the residual spatially independent noise, but it can have temporal autocorrelation, which may be modeled with an auto-regressive (AR) process such as AR(1). Generally, researchers do not have full knowledge of \mathbf{S}_0 or \mathbf{W}_0 , but may have regressors (such as the head motion time course) which accounts for some variance in \mathbf{S}_0 . Eq. 13 defines the conditional probability of the data in each voxel given \mathbf{S} , \mathbf{W} , \mathbf{S}_0 , \mathbf{W}_0 and the parameters θ of the AR process, e.g., $p(X^{(v)} | \mathbf{S}, \mathbf{W}^{(v)}, \mathbf{S}_0, \mathbf{W}_0^{(v)}, \theta^{(v)})$ for voxel v .

When cosine angle $\alpha_{i,j}$ is used as a measure of similarity between pat-

terns W_i and W_j (row vectors of \mathbf{W}), $\cos \alpha_{i,j} = \frac{W_i W_j^T}{\sqrt{W_i W_i^T} \sqrt{W_j W_j^T}}$. If the activation profile of each voxel $W^{(v)}$ is a sample from a multi-variate distribution, then $\mathbb{E}[W_i W_j^T]$ is the covariance between the dimensions i and j of this distribution[68]. By estimating the covariance structure U_W of \mathbf{W} , one can obtain the cosine angle between patterns as a similarity measure. Therefore, the relation between unknown neural patterns and their similarity is modeled by assuming that each column of \mathbf{W} is a sample drawn from a multivariate distribution with its covariance matrix being U_W :

$$W^{(v)} \sim N(0, U_W) \quad (14)$$

This specifies the form of conditional probability of $W^{(k)}$ given U_W : $p(W^{(k)}|U_W)$. The two-stage generating model from covariance structure through activity patterns to fMRI data is depicted in Fig. 5B.

- *Solving the model: inferring covariance structure of unknown neural patterns directly from data*

After the probabilistic graphical model is built and the conditional probability distribution corresponding to each edge is specified, one can derive the likelihood $p(\mathbf{X}|U_W)$. This can be achieved after marginalizing the intermediate variables such as \mathbf{W} and other unknown quantities that \mathbf{X} 's distribution is conditioned on (\mathbf{S}_0 is determined through an iterative fitting procedure as in [17]). Then maximizing this likelihood yields the maximum likelihood estimation \hat{U}_W of U_W . Finally, the cosine angles between \mathbf{W} can be obtained as the correlation matrix corresponding to the covariance matrix \hat{U}_W .

- *Application: reducing spurious similarity structure*

Maximizing the likelihood $p(\mathbf{X}|U_W)$ while marginalizing unknown intermediate variables and uninteresting variables is a principled approach to infer the latent variable U_W . An alternative pipeline-oriented approach is to instead first calculate $\hat{\mathbf{W}}$ as estimates of the unknown patterns \mathbf{W} from the data by regressing \mathbf{X} against \mathbf{S} , and then calculate the similarity among rows of $\hat{\mathbf{W}}$. This approach, however, has been shown [16–18, 69] to introduce spurious similarity structure unrelated to the neural activity corresponding to the task of interest. The reason is that although the regression provides unbiased estimates $\hat{\mathbf{W}}$ of the neural patterns, the covariance of $\hat{\mathbf{W}}$ is not the same as the covariance of \mathbf{W} : $\hat{\mathbf{W}}$ is contaminated by noise with specific covariance structure introduced by the regression procedure. The noise itself originates from the task-unrelated fluctuation in fMRI data. The regression procedure,

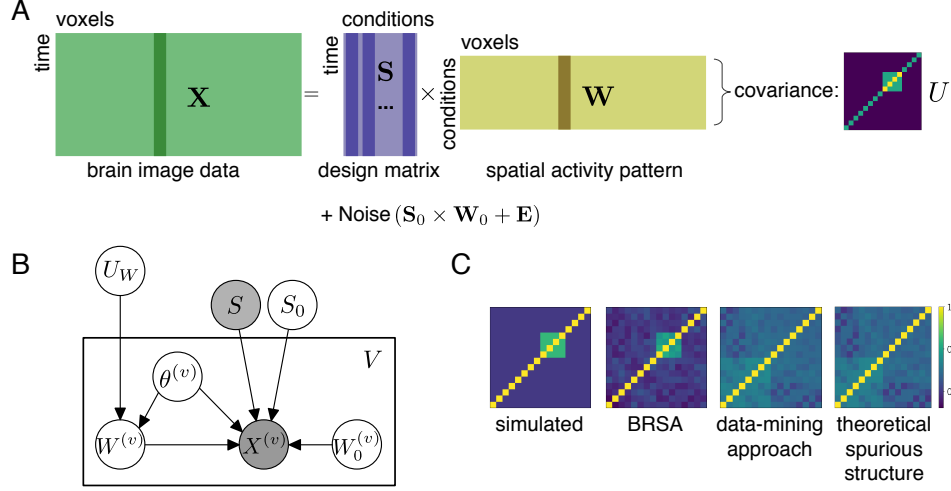


Figure 5: A) BRSA assumes a similar factor model as SRM and (H)TFA. To capture both spatial and temporal correlation in residual noise, the noise is further modeled by a factor decomposition of spatially correlated noise plus spatially independent noise. Additionally, each column of the weight matrix \mathbf{W} (activation patterns) are assumed to share the same covariance structure, which underlies the similarity between patterns. B) Probabilistic graphical model for BRSA. The rectangular plate is repeated for each voxel. Variables within the plate are voxel-specific and those outside the plate are shared by all voxels. U_W is the target to estimate but is indirectly related to \mathbf{X} through unknown patterns \mathbf{W} . To infer U_W , other unknown variables are either marginalized or (in the case of \mathbf{S}_0) determined through an iterative fitting procedure (see [17]) C) The simulated similarity structure, the similarity structures recovered by BRSA, by correlation of point estimates of \mathbf{W} (data-mining approach) and the theoretical spurious structure expected to be introduced by the design matrix \mathbf{S} when estimating $\hat{\mathbf{W}}$. B) and C) are adapted from [17]

at the same time of disentangling \mathbf{W} from \mathbf{X} , also “entangles” the noise into each row of $\hat{\mathbf{W}}$ in a way that depends on the correlational structure between different columns of \mathbf{S} . The covariance structure of the noise in $\hat{\mathbf{W}}$ can dominate the estimated similarity structure when signal-to-noise ratio is low [16, 17] (Fig. 5C). BRSA takes into account both the property of noise and uncertainty of intermediate variables \mathbf{W} , thus avoiding analyzing $\hat{\mathbf{W}}$ with structured noise.

Instead of directly inferring U_W from \mathbf{X} , one can alternatively assume that U_W is composed of the sum of a few theoretically-motivated candidate covariance structure, and estimate the mixture coefficient of each component covariance structure. This method is called Pattern Component Modeling

(PCM) [70, 71]. One can even impose hyperprior on the the mixing coefficients, and use variational Bayesian technique to infer them [72]. The introduction of hyperprior can incorporate additional prior assumption or knowledge of the data. These methods are both developed based on clear probabilistic graphical models. It is worth pointing out that in using these methods, in order to overcome the spurious similarity structure introduced by the design matrix \mathbf{S} , one needs to either directly model the data \mathbf{X} as in BRSA, or to model $\hat{\mathbf{W}}$ while explicitly taking into account the structure of the noise it carries.

Even if one takes the data mining approach, a correct understanding of the confounding effect of noise by analyzing a probabilistic graphical model is helpful for developing a better data mining procedure. For example, one can still approximate the covariance or distance structure based on the noisy patterns estimated from separate runs of experiment [18, 65]. This is because the noise of different runs are independent, and the expectation of the product of two independent zero-centered noises is zero. To see this, one needs to understand how data \mathbf{X} is generated from \mathbf{W} (13) and how the noise in this data generating process impacts $\hat{\mathbf{W}}$.

2.5. Modeling structured residuals

- Defining the problem: modeling spatiotemporal residuals in fMRI data

fMRI data has structure in both the spatial and temporal dimension, and this spatiotemporal consistency needs to be exploited (or at least, managed) in order to contend with this high-dimensional and noisy signal. This spatiotemporal structure exists both in the neural components corresponding to the effects of interest, and in the *residual* components corresponding to everything else going on. In the context of supervised regression models for fMRI, practitioners tend to worry about temporal structure in both signal (by convolving the predictors with a synthetic haemodynamic response function) and residual (by performing generalized least squares, or GLS, estimation wherein the temporal structure of the residuals is modeled, [e.g. 73]). More recent factor-analytic unsupervised approaches implicitly assume the signal of interest itself is likewise spatially or temporally structured due to their low-rank structure, for example the case of TFA (above) modeling brain networks as a linear combination (in time) of spatially contiguous factors. To the extent that they have modeled structure in the residuals, it has been in only the temporal or spatial dimensions (e.g., BRSA modeling residual temporal autocorrelation per-voxel).

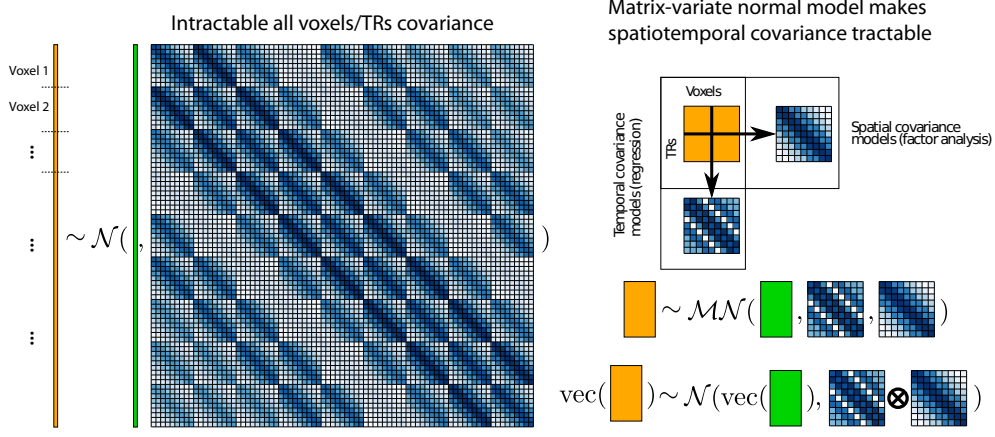


Figure 6: **Matrix normal models simultaneously model spatial and temporal residuals.** On the left is a schematic view of a vectorized data matrix, where each voxel’s time series is vertically concatenated (in orange), and the covariance of every voxel at every timepoint with every other voxel at every other timepoint is modeled. Modeling all of these elements independently is intractable, and some structure needs to be imposed – in this case, kronecker-separable structure. On the right is the un-vectorized data matrix (orange rectangle), and its spatial and temporal covariances on the right and bottom. A matrix-normal distribution with the mean (green rectangle) and row/column covariances on the right is equivalent to the large structure on the left, but can be much more tractable to estimate.

- *Making assumptions: structured, separable residuals*

As noted above, both the fMRI signal and residual are autocorrelated in both space and time; thus, modeling the residual structure in both dimensions is needed. This is not tractable in the general case, as it effectively means modeling the covariance between every voxel at every timepoint with every other voxel at every other timepoint. A simplifying assumption that permits modeling residuals in both space and time is that the spatial residuals of all time points have the same distribution, and the temporal residuals of all voxels likewise have the same distribution (for an illustration, see Fig. 6). This *separable* residuals assumption has been made in a GLS framework by Katanoda et al. [74] and factor-analytic framework by Shvartsman et al. [75]. A similar approach has been taken to modeling the entire dataset (rather than residuals only) in both neuroimaging [e.g. 76, 77] and elsewhere in the *multitask learning* community [e.g 78–82]. Once separability is assumed, theoretically motivated structure could be placed on the individual

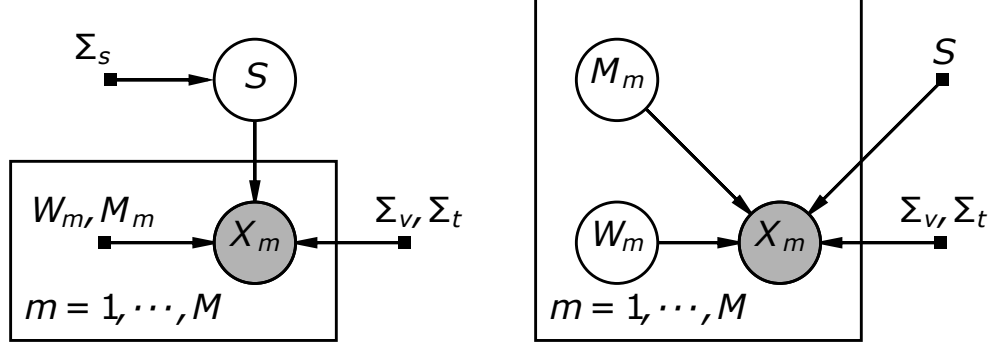


Figure 7: **Plate diagrams for matrix-normal shared response model.** In the matrix-normal notation one can see that there are two possible formulations for an SRM-type model: one which integrates over the shared timecourse (as SRM does), and one which integrates over the subject-specific weightings while removing the orthonormality assumption on \mathbf{W}_m (this is termed ‘dual probabilistic SRM’ or DP-SRM by analogy to dual probabilistic PCA, which makes the same extension to PCA [83]). In both cases, the brain image data $X_m \in \mathbb{R}^{V \times T}$ is observed from subject m , $m = 1 : M$. As in conventional SRM, each observation (now represented as the full data matrix) is a linear combination of subject-specific latent factors. In regular MN-SRM (left), the time-course \mathbf{S} is treated as a latent variable that is integrated over and the mean \mathbf{M}_m and weight vector \mathbf{W}_m are treated as (hyper)parameters that need to be estimated. In DP-SRM (right), the weight vector and mean matrix are treated as latent variables and integrated over whereas the shared timecourse is treated as a (hyper)parameter to estimate. Note how in contrast to Fig. 2, there is no plate denoting independence between timepoints, since their covariance is now modeled. Shaded nodes: observations, unshaded nodes: latent variables, and black squares: parameters.

spatial and temporal residual covariances, for example autoregressive in time (as in BRSA, above) and smooth in space (as in DRD, above).

- *Translating assumptions to a graphical model: matrix-normal*

The informal claim of separability above is denoted by defining Σ_{all} to be equal to the kronecker product of a spatial and temporal residual covariance, $\Sigma_{all} := \Sigma_t \otimes \Sigma_v$. The kronecker product is a generalization of the vector outer product to matrices, and precisely performs the weighted tiling illustrated in Fig. 6. Using this notation, we define the matrix-variate normal distribution, a distribution over matrices parameterized by a mean matrix and both row and column covariances. We denote matrices drawn from this distribution as

$\mathbf{X} \sim \mathcal{MN}_{m,n}(\mathbf{M}, \mathbf{R}, \mathbf{C})$, with mean $\mathbf{M} \in \mathbb{R}^{m \times n}$, row covariance $\mathbf{R} \in \mathbb{R}^{m \times m}$ and column covariance $\mathbf{C} \in \mathbb{R}^{n \times n}$. It has the following density:

$$\begin{aligned} \log p(\mathbf{X} \mid \mathbf{M}, \mathbf{R}, \mathbf{C}) = & -2 \log mn - m \log |\mathbf{C}| \\ & - n \log |\mathbf{R}| - \text{Tr} [\mathbf{C}^{-1}(\mathbf{X} - \mathbf{M})^\top \mathbf{R}^{-1}(\mathbf{X} - \mathbf{M})]. \end{aligned} \quad (15)$$

The above notation is equivalent to denoting $\text{vec}(\mathbf{X}) \sim \mathcal{N}(\text{vec}(\mathbf{M}), \mathbf{C} \otimes \mathbf{R})$, where \otimes is the kronecker product and vec is the vectorization operator. If the column covariance \mathbf{C} is the identity matrix, the expression reduces to the multivariate density summed over column dimension. We can use this notation to write, for example, a separable-residual model SRM model:

$$\mathbf{S} \sim \mathcal{MN}(0, \Sigma_s, \mathbf{I}) \quad (16)$$

$$\mathbf{X}_m \mid \mathbf{S} \sim \mathcal{MN}(\mathbf{W}_m \mathbf{S} + \mathbf{M}_m, \Sigma_v, \Sigma_t), \quad (17)$$

where Σ_v and Σ_t are spatial and temporal residual covariances and the remaining parameters are as defined above. In contrasting the diagram in Fig. 7 one can see the disappearance of the plate iterating over timepoints, since now temporal residuals are modeled. In this view, we can also see a similar model in which the prior on \mathbf{W}_m is modeled instead:

$$\mathbf{W}_m \sim \mathcal{MN}(0, \mathbf{I}, \Sigma_w) \quad (18)$$

$$\mathbf{X}_m \mid \mathbf{S} \sim \mathcal{MN}(\mathbf{W}_m \mathbf{S} + \mathbf{M}_m, \Sigma_v, \Sigma_t), \quad (19)$$

In this view, which Shvartsman et al. label dual probabilistic SRM (DP-SRM) by analogy to dual probabilistic PCA [83], \mathbf{W}_m can no longer be modeled as orthonormal but can now be integrated over with a gaussian prior, estimating substantially fewer parameters. Similar modification can be performed on other factor models [75].

- Solving the model

While simply estimating all parameters by gradient descent is theoretically possible, a more practical approach is to marginalize over nuisance parameters, and estimate only the parameters of interest. Marginalization in the multivariate normal setting with gaussian priors is well-known [84], but the separable covariance formulation introduces some new inference challenges: marginalization yields a non-separable marginal likelihood, naive computation of which would require inverting a matrix of dimension $vt \times vt$ for v voxels and t , which is intractable for fMRI data. However,

Rakitsch et al. [81] provide an efficient method for computing this likelihood by exploiting the compatibility between diagonalization and the kronecker product. If the spatial residual matrix itself needs to be separable (e.g. for efficiently modeling whole-brain spatial residuals by separating them in the x, y, and z dimensions), [75] show that particular assumptions about prior covariances can likewise render the marginal separable (and thus tractable). Once the marginal likelihood can be computed efficiently, standard gradient-based techniques can be used for estimation. For even greater speed, Shvartsman et al. [75] derive an expectation-conditional-maximization algorithm for maximizing the marginal likelihood by coordinate ascent (though they only do so for matrix-normal SRM).

Applications and benefits

In the case of the fMRI GLM, Katanoda et al. [74] validate the separable-residuals model on synthetic data, as well as on a finger-tapping experiment. There, they demonstrate that the separable model recovers larger activations more closely focused around the expected motor regions. Additionally, the separable model provided the best fit to the data out of the models considered (which included models that did not include any residual structure and those that included temporal structure only). In the case of factor models, Shvartsman et al. [75] show that the separable model can be substantially faster to estimate than a model that includes voxel-specific temporal residuals (as in the case of BRSA vs MN-RSA) and can achieve lower error while retaining BRSA’s conservative behavior under the null. A separable variant of SRM achieves lower out-of-sample reconstruction error for new subjects than conventional SRM, though this reduced error does not seem to translate to improved feature extraction for brain decoding.

3. Discussion

In this article, we use five computational tools developed for different goals in fMRI research to illustrate how to build probabilistic graphical model to address important questions arising in neural imaging studies. These methods also illustrate how the probabilistic graphical model[24], which stands at the center of all the methods, can accommodate domain knowledge and known properties of the data and facilitate aggregating information over larger datasets. These features allow us to mitigate the limitations in fMRI data: high dimensionality (many voxels), low sample size in single subject,

heterogeneity across subjects and complex noise with high magnitude. The model-based approach helps ensure the faithfulness of an algorithm to its original purpose and provides flexibility in model building.

To tackle the limits of high dimensionality and low sample size, SRM[30] uses shared latent response as its core assumption, which allows aggregating data from multiple subjects; HTFA [38] uses hierarchical model across subjects to discover common nodes in many brains. By utilizing big data across many subjects, both methods essentially increase the sample size to discover common structure in the data. In addition, the low-rank factor model underlying both methods reduce the model complexity, thus mitigating overfitting.

In aggregating data, both SRM and (H)TFA tolerate the heterogeneity of data across subjects, but in slightly different ways: SRM assumes different spatial weight matrices across subjects while HTFA allows the spatial location of the same node in different subjects to vary. Similarly, an extension of BRSA, the Group BRSA[17] allows spatial patterns to differ across subjects.

An alternative way to mitigate high dimensionality and low sample size is to introduce domain knowledge which trades off between bias and variance in parameter estimation. The three-dimensional Gaussian kernel in (H)TFA [38, 39] can be considered as adopting the belief that fMRI activations are smooth and local. DRD[46] introduces similar domain knowledge (region sparsity) to tackle the problem by resorting to a Gaussian Process prior on the log of decoding weight variance. This prior allows the weights to have more flexible spatial patterns than Gaussian blobs. Although not reviewed in this article, the method of estimating population receptive field [85] and more generally, the encoding model approach [86] essentially also bring in domain knowledge of neural tuning properties in modeling fMRI data.

Aggregating more data and introducing domain knowledge both essentially reduce the impact of high noise in fMRI data. BRSA and kronecker-separable factor model variants [75] go one step further by explicitly modeling the spatial and temporal correlation structure in noise. BRSA separates the spatially correlated and independent noise components and models the former with a factor model, allowing for a more complex correlation structure. Matrix normal assumes separability of the whole data covariance structure into one corresponding to spatial covariance and one corresponding to temporal covariance, largely reducing the number of free parameters while still being able to capture the major structure in noise. Explicitly modeling the noise structure helps reduce bias in estimation arising from the mismatch

between an overly simplified noise assumption and the complex property of noise in the data.

In addition to tackling the limitation in fMRI to increase the power for discovering meaningful information in the data, one advantage of the model-based approach is its faithfulness to the original goal of a research. This is illustrated in the case of BRSA, where a data-mining approach may overlook the difference between the output of a previous analysis procedure and the true quantity of data that the procedure attempts to estimate, and may introduce spurious results. Probabilistic graphical models allow for simulation of data according to the model and verification of the inference algorithm. This is an advantage not easily achieved by analysis procedures developed without an explicit graphical model.

The model-based approach to neuroimaging analysis also offers the flexibility of combining advantages of different models and tailoring models for new application domains. This has been illustrated by the extensions of SRM to several variants that utilize partial labels of data[35] or datasets partially sharing subjects[34]. Likewise, it is illustrated in the development of separable-covariance variants of existing models [75]. It is an interesting future research direction to develop new tools that combine the advantage of the existing model-based methods, including the models reviewed here. Understanding the commonality among models is the first step towards integrating them. This is the reason we intentionally use the same notation and matrix orientation of data matrix in this paper to help readers see the commonality among these methods. Furthermore, several of the tools in this article are available in the same open source package *Brain Imaging Analysis Kit* (*BrainIAK*) [87], which makes it easier for tool developers to understand how the computational models and inference algorithms ultimately turn into functioning code and to draw inspiration from these tools.

In the new era of big data for neuroscience[88–90], facilitating data sharing is obviously one of the most important effort for making big data analysis possible[91–94]. One step further, developing computational models that derive insights from the big data is another key for the field of neuroscience to benefit from the increasing data size, which should also be in synergy with development of theory of the essence of the neural computation[95–97]. We suggest the process of future method development should place model building as a central focus.

4. Acknowledgement

MBC is supported by National Institute of Drug Abuse award R01DA042065

References

- [1] S. Ogawa, T.-M. Lee, A. R. Kay, D. W. Tank, Brain magnetic resonance imaging with contrast dependent on blood oxygenation, *Proceedings of the National Academy of Sciences* 87 (1990) 9868–9872.
- [2] J. Belliveau, D. Kennedy, R. McKinstry, B. Buchbinder, R. Weisskoff, M. Cohen, J. Vevea, T. Brady, B. Rosen, Functional mapping of the human visual cortex by magnetic resonance imaging, *Science* 254 (1991) 716–719.
- [3] R. B. Buxton, The physics of functional magnetic resonance imaging (fmri), *Reports on Progress in Physics* 76 (2013) 096601.
- [4] D. J. Heeger, D. Ress, What does fmri tell us about neuronal activity?, *Nature Reviews Neuroscience* 3 (2002) 142.
- [5] K. J. Friston, A. P. Holmes, K. J. Worsley, J.-P. Poline, C. D. Frith, R. S. Frackowiak, Statistical parametric maps in functional imaging: a general linear approach, *Human brain mapping* 2 (1994) 189–210.
- [6] R. W. Cox, Afni: software for analysis and visualization of functional magnetic resonance neuroimages, *Computers and Biomedical research* 29 (1996) 162–173.
- [7] S. M. Smith, M. Jenkinson, M. W. Woolrich, C. F. Beckmann, T. E. Behrens, H. Johansen-Berg, P. R. Bannister, M. De Luca, I. Drobnjak, D. E. Flitney, et al., Advances in functional and structural mr image analysis and implementation as fsl, *Neuroimage* 23 (2004) S208–S219.
- [8] K. N. Kay, A. Rokem, J. Winawer, R. F. Dougherty, B. A. Wandell, Glmddenoise: a fast, automated technique for denoising task-based fmri data, *Frontiers in neuroscience* 7 (2013).
- [9] R. E. Kelly Jr, G. S. Alexopoulos, Z. Wang, F. M. Gunning, C. F. Murphy, S. S. Morimoto, D. Kanellopoulos, Z. Jia, K. O. Lim, M. J. Hoptman, Visual inspection of independent components: defining a

- procedure for artifact removal from fmri data, *Journal of neuroscience methods* 189 (2010) 233–245.
- [10] R. H. Pruim, M. Mennes, D. van Rooij, A. Llera, J. K. Buitelaar, C. F. Beckmann, Ica-aroma: A robust ica-based strategy for removing motion artifacts from fmri data, *Neuroimage* 112 (2015) 267–277.
 - [11] G. H. Glover, T.-Q. Li, D. Ress, Image-based method for retrospective correction of physiological motion effects in fmri: Retroicor, *Magnetic Resonance in Medicine: An Official Journal of the International Society for Magnetic Resonance in Medicine* 44 (2000) 162–167.
 - [12] K. J. Worsley, K. J. Friston, Analysis of fmri time-series revisited again, *Neuroimage* 2 (1995) 173–181.
 - [13] K. Gorgolewski, C. D. Burns, C. Madison, D. Clark, Y. O. Halchenko, M. L. Waskom, S. S. Ghosh, Nipype: a flexible, lightweight and extensible neuroimaging data processing framework in python, *Frontiers in neuroinformatics* 5 (2011) 13.
 - [14] O. Esteban, C. J. Markiewicz, R. W. Blair, C. A. Moodie, A. I. Isik, A. Erramuzpe, J. D. Kent, M. Goncalves, E. DuPre, M. Snyder, et al., fmriprep: a robust preprocessing pipeline for functional mri, *Nature methods* 16 (2019) 111.
 - [15] M. A. Lindquist, S. Geuter, T. D. Wager, B. S. Caffo, Modular preprocessing pipelines can reintroduce artifacts into fmri data, *Human brain mapping* 40 (2019) 2358–2376.
 - [16] M. B. Cai, N. W. Schuck, J. W. Pillow, Y. Niv, A bayesian method for reducing bias in neural representational similarity analysis, in: *Advances in Neural Information Processing Systems*, pp. 4951–4959.
 - [17] M. B. Cai, N. W. Schuck, J. W. Pillow, Y. Niv, Representational structure or task structure? bias in neural representational similarity analysis and a bayesian method for reducing bias, *PLoS computational biology* 15 (2019) e1006299.
 - [18] A. Alink, A. Walther, A. Krugliak, J. J. van den Bosch, N. Kriegeskorte, Mind the drift-improving sensitivity to fmri pattern information by accounting for temporal pattern drift, *bioRxiv* (2015) 032391.

- [19] J. E. Chen, H. Jahanian, G. H. Glover, Nuisance regression of high-frequency functional magnetic resonance imaging data: denoising can be noisy, *Brain connectivity* 7 (2017) 13–24.
- [20] K. Murphy, M. D. Fox, Towards a consensus regarding global signal regression for resting state functional connectivity mri, *Neuroimage* 154 (2017) 169–173.
- [21] K. Murphy, R. M. Birn, D. A. Handwerker, T. B. Jones, P. A. Bandettini, The impact of global signal regression on resting state correlations: are anti-correlated networks introduced?, *Neuroimage* 44 (2009) 893–905.
- [22] Z. S. Saad, S. J. Gotts, K. Murphy, G. Chen, H. J. Jo, A. Martin, R. W. Cox, Trouble at rest: how correlation patterns and group differences become distorted after global signal regression, *Brain connectivity* 2 (2012) 25–32.
- [23] N. Leonardi, D. Van De Ville, On spurious and real fluctuations of dynamic functional connectivity during rest, *Neuroimage* 104 (2015) 430–436.
- [24] D. Koller, N. Friedman, Probabilistic graphical models: principles and techniques, MIT press, 2009.
- [25] C. M. Bishop, Pattern recognition and machine learning, springer, 2006.
- [26] M. W. Woolrich, Bayesian inference in fmri, *NeuroImage* 62 (2012) 801–810.
- [27] M. W. Woolrich, S. Jbabdi, B. Patenaude, M. Chappell, S. Makni, T. Behrens, C. Beckmann, M. Jenkinson, S. M. Smith, Bayesian analysis of neuroimaging data in fsl, *Neuroimage* 45 (2009) S173–S186.
- [28] J. Talairach, Co-planar stereotaxic atlas of the human brain-3-dimensional proportional system, An approach to cerebral imaging (1988).
- [29] J. Mazziotta, A. Toga, A. Evans, P. Fox, J. Lancaster, K. Zilles, R. Woods, T. Paus, G. Simpson, B. Pike, et al., A probabilistic atlas and reference system for the human brain: International consortium for

brain mapping (icbm), *Philosophical Transactions of the Royal Society of London. Series B: Biological Sciences* 356 (2001) 1293–1322.

- [30] P.-H. C. Chen, J. Chen, Y. Yeshurun, U. Hasson, J. Haxby, P. J. Ramadge, A reduced-dimension fmri shared response model, in: *Advances in Neural Information Processing Systems*, pp. 460–468.
- [31] K. Vodrahalli, P.-H. Chen, Y. Liang, C. Baldassano, J. Chen, E. Yong, C. Honey, U. Hasson, P. Ramadge, K. A. Norman, et al., Mapping between fmri responses to movies and their natural language annotations, *Neuroimage* 180 (2018) 223–231.
- [32] J. V. Haxby, J. S. Guntupalli, A. C. Connolly, Y. O. Halchenko, B. R. Conroy, M. I. Gobbini, M. Hanke, P. J. Ramadge, A common, high-dimensional model of the representational space in human ventral temporal cortex, *Neuron* 72 (2011) 404–416.
- [33] H. Zhang, P.-H. Chen, J. Chen, X. Zhu, J. S. Turek, T. L. Willke, U. Hasson, P. J. Ramadge, A searchlight factor model approach for locating shared information in multi-subject fmri analysis, *arXiv preprint arXiv:1609.09432* (2016).
- [34] H. Zhang, P.-H. Chen, P. Ramadge, Transfer learning on fmri datasets, in: *International Conference on Artificial Intelligence and Statistics*, pp. 595–603.
- [35] J. S. Turek, T. L. Willke, P.-H. Chen, P. J. Ramadge, A semi-supervised method for multi-subject fmri functional alignment, in: *2017 IEEE International Conference on Acoustics, Speech and Signal Processing (ICASSP)*, IEEE, pp. 1098–1102.
- [36] N. B. Turk-Browne, Functional interactions as big data in the human brain, *Science* 342 (2013) 580–584.
- [37] M. Rubinov, O. Sporns, Complex network measures of brain connectivity: uses and interpretations, *NeuroImage* 52 (2010) 1059 – 1069.
- [38] J. Manning, X. Zhu, T. Willke, R. Ranganath, K. Stachenfeld, U. Hasson, D. Blei, K. Norman, A probabilistic approach to discovering dynamic full-brain functional connectivity patterns, *NeuroImage* 180 (2018) 243 – 52.

- [39] J. R. Manning, R. Ranganath, K. A. Norman, D. M. Blei, Topographic factor analysis: a Bayesian model for inferring brain networks from neural data, *PLoS One* 9 (2014) e94914.
- [40] A. J. O’Toole, F. Jiang, H. Abdi, N. Pénard, J. P. Dunlop, M. A. Parent, Theoretical, statistical, and practical perspectives on pattern-based classification approaches to the analysis of functional neuroimaging data, *Journal of cognitive neuroscience* 19 (2007) 1735–1752.
- [41] S. LaConte, S. Strother, V. Cherkassky, J. Anderson, X. Hu, Support vector machines for temporal classification of block design fmri data, *NeuroImage* 26 (2005) 317–329.
- [42] D. D. Cox, R. L. Savoy, Functional magnetic resonance imaging (fmri) brain reading: detecting and classifying distributed patterns of fmri activity in human visual cortex, *Neuroimage* 19 (2003) 261–270.
- [43] M. K. Carroll, G. A. Cecchi, I. Rish, R. Garg, A. R. Rao, Prediction and interpretation of distributed neural activity with sparse models, *NeuroImage* 44 (2009) 112–122.
- [44] V. Michel, A. Gramfort, G. Varoquaux, E. Eger, B. Thirion, Total variation regularization for fmri-based prediction of behavior, *IEEE transactions on medical imaging* 30 (2011) 1328–1340.
- [45] L. Grosenick, B. Klingenberg, K. Katovich, B. Knutson, J. E. Taylor, Interpretable whole-brain prediction analysis with graphnet, *NeuroImage* 72 (2013) 304–321.
- [46] A. Wu, O. Koyejo, J. Pillow, Dependent relevance determination for smooth and structured sparse regression, *Journal of Machine Learning Research* 20 (2019) 1–43.
- [47] M. E. Tipping, Sparse bayesian learning and the relevance vector machine, *The journal of machine learning research* 1 (2001) 211–244.
- [48] A. Tipping, A. Faul, Analysis of sparse bayesian learning, *Advances in neural information processing systems* 14 (2002) 383–389.
- [49] D. Wipf, S. Nagarajan, A new view of automatic relevance determination, in: J. Platt, D. Koller, Y. Singer, S. Roweis (Eds.), *Advances*

- in *Neural Information Processing Systems 20*, MIT Press, Cambridge, MA, 2008, pp. 1625–1632.
- [50] M. Sahani, J. F. Linden, Evidence optimization techniques for estimating stimulus-response functions, *Advances in neural information processing systems* (2003) 317–324.
 - [51] A. Schmolck, *Smooth Relevance Vector Machines*, Ph.D. thesis, University of Exeter, 2008.
 - [52] M. Park, J. W. Pillow, Receptive field inference with localized priors, *PLoS computational biology* 7 (2011) e1002219.
 - [53] R. M. Neal, *Bayesian learning for neural networks*, volume 118, Springer Science & Business Media, 2012.
 - [54] C. E. Rasmussen, Gaussian processes in machine learning, in: *Summer School on Machine Learning*, Springer, pp. 63–71.
 - [55] J. V. Haxby, M. I. Gobbini, M. L. Furey, A. Ishai, J. L. Schouten, P. Pietrini, Distributed and overlapping representations of faces and objects in ventral temporal cortex, *Science* 293 (2001) 2425–2430.
 - [56] R. Epstein, A. Harris, D. Stanley, N. Kanwisher, The parahippocampal place area: Recognition, navigation, or encoding?, *Neuron* 23 (1999) 115–125.
 - [57] E. Eger, J. Ashburner, J.-D. Haynes, R. J. Dolan, G. Rees, fmri activity patterns in human loc carry information about object exemplars within category, *Journal of cognitive neuroscience* 20 (2008) 356–370.
 - [58] J. J. DiCarlo, D. Zoccolan, N. C. Rust, How does the brain solve visual object recognition?, *Neuron* 73 (2012) 415–434.
 - [59] D. Marr, H. K. Nishihara, Representation and recognition of the spatial organization of three-dimensional shapes, *Proceedings of the Royal Society of London. Series B. Biological Sciences* 200 (1978) 269–294.
 - [60] R. N. Shepard, S. Chipman, Second-order isomorphism of internal representations: Shapes of states, *Cognitive psychology* 1 (1970) 1–17.

- [61] K. A. Ericsson, H. A. Simon, Verbal reports as data., *Psychological review* 87 (1980) 215.
- [62] N. Kriegeskorte, M. Mur, P. A. Bandettini, Representational similarity analysis-connecting the branches of systems neuroscience, *Frontiers in systems neuroscience* 2 (2008) 4.
- [63] A. C. Connolly, J. S. Guntupalli, J. Gors, M. Hanke, Y. O. Halchenko, Y.-C. Wu, H. Abdi, J. V. Haxby, The representation of biological classes in the human brain, *The Journal of Neuroscience* 32 (2012) 2608–2618.
- [64] M. C. Iordan, M. R. Greene, D. M. Beck, L. Fei-Fei, Basic level category structure emerges gradually across human ventral visual cortex, *Journal of cognitive neuroscience* 27 (2015) 1427–1446.
- [65] J. Diedrichsen, S. Provost, H. Zareamoghaddam, On the distribution of cross-validated mahalanobis distances, *arXiv preprint arXiv:1607.01371* (2016).
- [66] F. M. Ramírez, Representational confusion: the plausible consequence of demeaning your data, *bioRxiv* (2017) 195271.
- [67] H. Nili, C. Wingfield, A. Walther, L. Su, W. Marslen-Wilson, N. Kriegeskorte, A toolbox for representational similarity analysis, *PLoS computational biology* 10 (2014) e1003553.
- [68] J. Diedrichsen, N. Kriegeskorte, Representational models: A common framework for understanding encoding, pattern-component, and representational-similarity analysis, *PLoS computational biology* 13 (2017) e1005508.
- [69] L. Henriksson, S.-M. Khaligh-Razavi, K. Kay, N. Kriegeskorte, Visual representations are dominated by intrinsic fluctuations correlated between areas, *NeuroImage* 114 (2015) 275–286.
- [70] J. Diedrichsen, G. R. Ridgway, K. J. Friston, T. Wiestler, Comparing the similarity and spatial structure of neural representations: a pattern-component model, *Neuroimage* 55 (2011) 1665–1678.
- [71] J. Diedrichsen, A. Yokoi, S. A. Arbuckle, Pattern component modeling: A flexible approach for understanding the representational structure of brain activity patterns, *NeuroImage* (2017).

- [72] K. J. Friston, J. Diedrichsen, E. Holmes, P. Zeidman, Variational representational similarity analysis, *NeuroImage* (2019) 115986.
- [73] J. A. Mumford, T. Nichols, Modeling and inference of multisubject fMRI data, *IEEE Engineering in Medicine and Biology Magazine* 25 (2006) 42–51.
- [74] K. Katanoda, Y. Matsuda, M. Sugishita, A spatio-temporal regression model for the analysis of functional MRI data, *NeuroImage* 17 (2002) 1415–1428.
- [75] M. Shvartsman, N. Sundaram, M. Aoi, A. Charles, T. L. Willke, J. D. Cohen, Matrix-normal models for fMRI analysis, *International Conference on Artificial Intelligence and Statistics, AISTATS 2018* (2018) 1914–1923.
- [76] F. Bijma, J. C. De Munck, R. M. Heethaar, The spatiotemporal MEG covariance matrix modeled as a sum of Kronecker products, *NeuroImage* 27 (2005) 402–415.
- [77] B. Roś, F. Bijma, M. de Gunst, J. de Munck, A three domain covariance framework for EEG/MEG data, *NeuroImage* 119 (2014) 305–315.
- [78] E. Bonilla, K. M. Chai, C. Williams, Multi-task Gaussian Process Prediction, *Nips* 20 (2008) 153–160.
- [79] G. Skolidis, G. Sanguinetti, Bayesian Multitask Classification With Gaussian Process Priors, *IEEE Transactions on Neural Networks* 22 (2011) 2011–2021.
- [80] O. Stegle, C. Lippert, J. Mooij, N. D. Lawrence, K. Borgwardt, Efficient inference in matrix-variate Gaussian models with iid observation noise, *Advances in Neural Information Processing Systems* 24 (NIPS 2011) (2011) 630–638.
- [81] B. Rakitsch, C. Lippert, K. Borgwardt, O. Stegle, It is all in the noise: Efficient multi-task Gaussian process inference with structured residuals, *Advances in Neural Information Processing Systems* (2013) 1466–1474.
- [82] K. Greenewald, A. O. Hero, Robust Kronecker Product PCA for Spatio-Temporal Covariance Estimation, *IEEE Transactions on Signal Processing* 63 (2015) 6368–6378.

- [83] N. D. Lawrence, Probabilistic non-linear Principal Component Analysis with Gaussian Process Latent Variable Models, *Journal of Machine Learning Research* 6 (2005) 1783–1816.
- [84] C. M. Bishop, *Pattern Recognition and Machine Learning*, Springer-Verlag New York, Inc., Secaucus, NJ, USA, 2006.
- [85] S. O. Dumoulin, B. A. Wandell, Population receptive field estimates in human visual cortex, *Neuroimage* 39 (2008) 647–660.
- [86] T. Naselaris, K. N. Kay, S. Nishimoto, J. L. Gallant, Encoding and decoding in fmri, *Neuroimage* 56 (2011) 400–410.
- [87] M. Kumar, C. T. Ellis, Q. Lu, H. Zhang, M. Capota, T. L. Willke, P. J. Ramadge, N. Turk-Browne, K. Norman, Brainiak tutorials: user-friendly learning materials for advanced fmri analysis (2019).
- [88] E. Landhuis, *Neuroscience: Big brain, big data*, 2017.
- [89] E. R. Kandel, H. Markram, P. M. Matthews, R. Yuste, C. Koch, Neuroscience thinks big (and collaboratively), *Nature Reviews Neuroscience* 14 (2013) 659.
- [90] J. D. Van Horn, A. W. Toga, Human neuroimaging as a big data science, *Brain imaging and behavior* 8 (2014) 323–331.
- [91] R. A. Poldrack, K. J. Gorgolewski, Making big data open: data sharing in neuroimaging, *Nature neuroscience* 17 (2014) 1510.
- [92] S. Choudhury, J. R. Fishman, M. L. McGowan, E. T. Juengst, Big data, open science and the brain: lessons learned from genomics, *Frontiers in human neuroscience* 8 (2014) 239.
- [93] K. Gorgolewski, O. Esteban, G. Schaefer, B. Wandell, R. Poldrack, Openneuro: a free online platform for sharing and analysis of neuroimaging data, *Organization for Human Brain Mapping. Vancouver, Canada* 1677 (2017).
- [94] K. J. Gorgolewski, T. Auer, V. D. Calhoun, R. C. Craddock, S. Das, E. P. Duff, G. Flandin, S. S. Ghosh, T. Glatard, Y. O. Halchenko, et al., The brain imaging data structure, a format for organizing and describing outputs of neuroimaging experiments, *Scientific Data* 3 (2016) 160044.

- [95] J. D. Cohen, N. Daw, B. Engelhardt, U. Hasson, K. Li, Y. Niv, K. A. Norman, J. Pillow, P. J. Ramadge, N. B. Turk-Browne, et al., Computational approaches to fmri analysis, *Nature neuroscience* 20 (2017) 304.
- [96] T. J. Sejnowski, P. S. Churchland, J. A. Movshon, Putting big data to good use in neuroscience, *Nature neuroscience* 17 (2014) 1440.
- [97] D. Bzdok, B. T. Yeo, Inference in the age of big data: Future perspectives on neuroscience, *Neuroimage* 155 (2017) 549–564.